

Emergence of Bloch oscillations in one-dimensional systems

Bogdan Stefan Popescu*

Max Planck Institute for the Physics of Complex Systems, Noethnitzer Strasse 38, 01187 Dresden, Germany

Alexander Croy†

Institute for Materials Science and Max Bergmann Center of Biomaterials, Dresden University of Technology, 01062 Dresden, Germany

(Received 25 January 2017; published 27 June 2017)

Electrons in periodic potentials exhibit oscillatory motion in the presence of an electric field. Such oscillations are known as Bloch oscillations. In this article we theoretically investigate the emergence of Bloch oscillations for systems where the electric field is confined to a finite region, like in typical electronic devices. We use a one-dimensional tight-binding model within the single-band approximation to numerically study the dynamics of electrons after a sudden switching-on of the electric field. We find a transition from a regime with direct current to Bloch oscillations when increasing the system size or decreasing the field strength. We propose a pump-probe scheme to observe the oscillations by measuring the accumulated charge as a function of the pulse length.

DOI: [10.1103/PhysRevB.95.235433](https://doi.org/10.1103/PhysRevB.95.235433)**I. INTRODUCTION**

Since the seminal works of Bloch [1] and Zener [2] it is well established that electrons in a periodic potential exhibit oscillatory motion after a static electric field is switched on (for a review see Ref. [3]). The periodic motion of the electrons in this context is also known as Bloch oscillations (BOs). The period of the oscillations is given by $T_B = h/F_0 a$, where h is Planck's constant, a is the lattice spacing, and F_0 is the electric field strength. In practice the BOs are typically suppressed by loss of coherence due to collisions, which makes it challenging to observe BOs in experiments. Over the last decades BOs have been found and characterized in various systems, for instance in semiconductor superlattices [4–8], ultracold atomic gases [9–11], or photonic waveguide arrays [12–14].

Also on the theoretical side there has been considerable interest in studying BOs. For instance, their interplay with disorder [15,16], light [17,18], interactions [19–21], or other degrees of freedom [22] has been investigated. In many cases, the essential physics can already be captured using a single-band approximation and considering a one-dimensional (1D) tight-binding (TB) chain [23].

In most theoretical studies, BOs have been considered in infinite systems. Here we investigate the emergence of BOs in a system where the electric field is confined to a finite-size region. This scenario corresponds to the typical setup of a device coupled to electronic leads. If the device is sufficiently small, one expects to find a direct current (dc) in the steady state. On the other hand, if the system is infinitely large, one will get BOs as discussed above. In this article we study the transition between the two regimes by increasing the device size and by changing the magnitude of the applied electric field. An important issue is the detection of BOs in such devices. We propose a pump-probe scheme, which uses the rising and falling flanks of a nearly rectangular pulse, to obtain information about the internal dynamics and BOs.

As in Ref. [23] we consider a 1D TB system and neglect the influence of electron-electron interactions. To account for the time dependence of the electric field, we use a recently developed numerical method [24], which is based on the time-dependent nonequilibrium Green's function (TDNEGF) formalism [25,26] in combination with an auxiliary-mode expansion [27]. This approach has already been successfully applied to study time-dependent nanoelectronics [28–34] and it allows us to obtain the time-dependent currents and occupations during and after the pulse has been applied. This information is then used to characterize the spatiotemporal evolution of the electrons in the device.

The article is organized as follows: Section II gives details on the specific setup and introduces the numerical scheme used in our study. Section III elaborates on the main results, whereas Sec. IV concludes the present work.

II. TRANSPORT SETUP AND METHOD

The setup consists of a generic one-dimensional (1D) system which is described as a tight-binding chain. The system as well as reservoirs sites are coupled to their nearest neighbors (see Fig. 1). Thus, the Hamiltonian in second quantization is expressed as

$$H(t) = \sum_{n=-\infty}^{\infty} \varepsilon_n(t) c_n^\dagger c_n - \gamma \sum_{n=-\infty}^{\infty} (c_n^\dagger c_{n+1} + c_{n+1}^\dagger c_n), \quad (1)$$

$$\text{with } \varepsilon_n(t) = \begin{cases} \varepsilon_L(t), & \text{if } n \leq 0 & \text{(left lead),} \\ \varepsilon_{Dn}(t), & \text{if } 1 \leq n \leq N & \text{(device),} \\ \varepsilon_R(t), & \text{if } n > N & \text{(right lead).} \end{cases}$$

Here $\varepsilon_n(t)$ denotes the time-dependent site energies for device and leads, γ is the intersite hopping parameter, whereas c_n^\dagger (c_n) creates (annihilates) an electron at site n . The device region consists of sites $1, \dots, N$, while the left (right) lead is defined by sites $n < 1$ ($n > N$).

To study the time evolution of the device, we employ a numerical method based on the TDNEGF formalism, which was recently put forward in Ref. [24]. The time evolution of

*Present address: Department of Physics and Astronomy, University of Delaware, Newark, DE 19716-2570, USA; popescu@udel.edu

†alexander.croy@tu-dresden.de

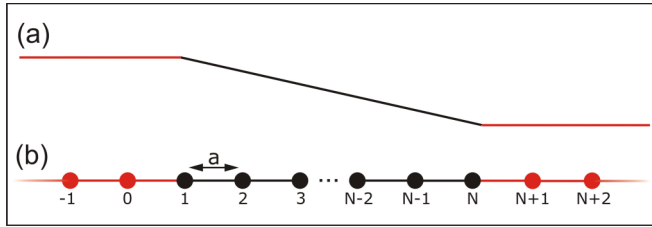


FIG. 1. (a) Sketch of the field-induced site energies (constant in the leads, linearly decreasing in the system). (b) Sketch of the TB chain: the system sites (orbitals) depicted in black (indexed from 1 to N) are connected to left and right leads depicted in red.

the reduced density operator (RDO) σ is given by

$$i\hbar \frac{d}{dt} \sigma(t) = [\mathbf{H}_D(t), \sigma(t)] + i \sum_{\alpha \in \{L, R\}} [\Pi_{\alpha}(t) + \Pi_{\alpha}^{\dagger}(t)]. \quad (2)$$

Here $\mathbf{H}_D(t)$ denotes the device part of the Hamiltonian, whereas the current matrices $\Pi_{\alpha}(t)$ are given by another set of equations (for details see Appendix B and Refs. [24,27]). These allow it to compute the time-resolved current from reservoir $\alpha = L, R$ into the device via

$$J_{\alpha}(t) = \frac{2e}{\hbar} \text{ReTr}\{\Pi_{\alpha}(t)\}. \quad (3)$$

Note that this propagation scheme solves Eq. (2) in time domain. Hence one has access to time-resolved quantities like the instantaneous occupations given by $\sigma_{ii}(t)$, $i = 1, \dots, N$. Moreover, the partial current between next neighboring system sites is given in terms of matrix elements of the RDO by

$$J_{i+1,i}(t) = i \frac{e\gamma}{\hbar} [\sigma_{i+1,i}(t) - \sigma_{i,i+1}(t)]. \quad (4)$$

In the following we use the intersite hopping parameter γ as the unit of energy. In semiconductor superlattices [5–8], which are made of alternating layers of semiconductor materials with small and large band gaps, one finds $\gamma \approx 20$ meV and the typical lattice parameter is $a \approx 100$ Å. The magnitude of the electric field is then given in units of $\gamma/ea \approx 20$ keV/cm. The unit of time is $\hbar/\gamma \approx 0.2$ ps.

III. RESULTS AND DISCUSSION

A. Steady-state dynamics

In this section we analyze the occurrence of Bloch oscillations in response to the sudden switching-on of an external electric field. Initially, the system is in equilibrium with the reservoirs at $\mu = \mu_L = \mu_R = -\gamma$ and $k_B T = 10^{-2}\gamma$. An electric field (or equivalently a bias voltage) is suddenly switched on at $t = t_0$ and it is assumed that the voltage drop is linear across the device. Hence, the time dependence of the site energies is given by $\varepsilon_i(t) = aF(t)[(N+1)/2 - i]$ and $\varepsilon_L = -\varepsilon_R = aF(t)(N-1)/2$, where $F(t) = F_0\{1 + \text{erf}[(t - t_0)/t_r]\}/2$ is the instantaneous force due to an electric field $F(t)/e$ and erf is the error function. The rise time of the electric field is given by t_r (in all present simulations $t_r = 10\hbar/\gamma$).

First, in Fig. 2 we explore the steady-state behavior. To this end we calculate the time average of the current through the center of the system $\langle J_{\text{cent.}}(t) \rangle$, where $J_{\text{cent.}}(t) \equiv J_{N/2+1, N/2}(t)$.

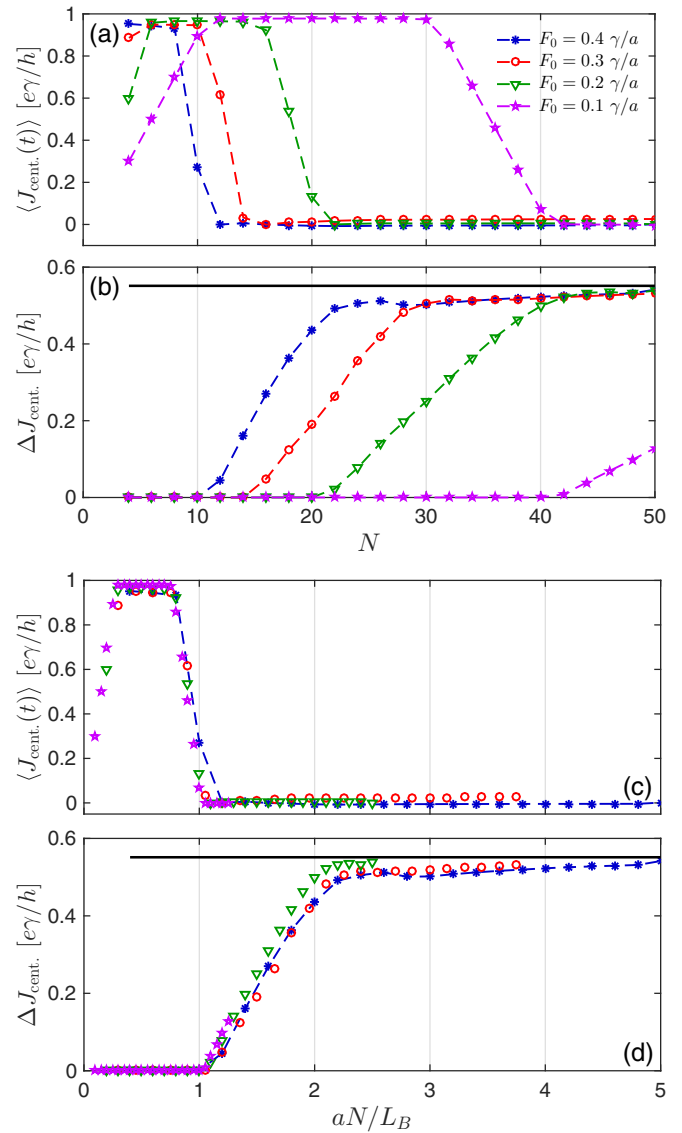


FIG. 2. (a) Time average of the electronic current in the center of the system $J_{\text{cent.}}$ and (b) half range of mean absolute deviation for $J_{\text{cent.}}$, both computed as function of system size (N) for several values of field magnitude (F_0). (c) and (d) The same data as (a) and (b) but with the system size being scaled by the Bloch length L_B . Dashed lines are guides to the eye. The solid black lines indicate the current amplitude according to Eq. (A4).

As one can see in Fig. 2(a), for small system sizes N there is a linear increase of the average current with system size, which eventually saturates to a maximal value. For larger N , there is a transition regime, where $\langle J_{\text{cent.}}(t) \rangle$ monotonously decreases. For even larger N the average current becomes identically zero. This behavior can readily be understood by noting that the bandwidth of the leads is 4γ and the bias voltage becomes $eV = \varepsilon_L - \varepsilon_R = F_0 a(N-1)$ for $t - t_0 \gg t_r$. The current increases as $J = (e/\hbar)V$ up to the point where the lower band edge of the left lead raises over the chemical potential in the right lead, i.e., for $eV = 2\gamma + \mu$. Now, all occupied states in the left lead have corresponding empty states in the right lead. This changes when the chemical potential

in the left lead raises above the upper band edge in the right lead, i.e., for $eV = 2\gamma - \mu$. The current drops linearly to zero, $J = (e/h)(4\gamma - eV)$, since at $eV = 4\gamma$ the bands of the leads do not overlap any longer.

In addition, in Fig. 2(b) we show the half range of the mean absolute deviation for $J_{\text{cent.}}$. This quantity is defined as

$$\Delta J_{\text{cent.}} = \{\max[J_{\text{cent.}}(t) - \langle J_{\text{cent.}}(t) \rangle] - \min[J_{\text{cent.}}(t) - \langle J_{\text{cent.}}(t) \rangle]\}/2. \quad (5)$$

In the range where the average current is nonvanishing, we find that $\Delta J_{\text{cent.}}$ is zero. This implies that a dc is flowing in the steady state as long as $F_0 a(N-1) \leq 4\gamma$. From Fig. 2(b) one sees that $\Delta J_{\text{cent.}} > 0$ if the system size is further increased and the average current vanishes. This behavior is consistent with an oscillating current.

The transition from dc towards an oscillatory regime can be qualitatively explained by the emergence of BOs. Specifically, there is a typical length scale of BOs, which is given by the Bloch length [23]

$$L_B = \frac{4\gamma}{F_0}, \quad (6)$$

where 4γ is the bandwidth of a 1D-TB chain. This means that the system size needs be greater than the Bloch length, in order to observe oscillatory behavior. This argument is supported by Figs. 2(c) and 2(d), where the scaling of the data by the Bloch length is shown.

B. Time-resolved dynamics

To explore the effect in more detail, we fix the system size to $N = 50$ and examine the time-dependent response for different external field magnitudes. Specifically, the time dependence of the site occupation numbers and the currents obtained by our method are shown in Fig. 3. Each triple-block plot shows the dynamics computed for a value of F_0 , namely $F_0 = 0.05\gamma/a$, $0.1\gamma/a$ and $0.2\gamma/a$. Note that in each block displayed are from top to bottom: the site occupation number $\sigma_{ii}(t)$ (given by the diagonal elements of the RDO), the partial currents between neighboring sites $J_{i,i+1}(t)$, as well as the current through the center of the system $J_{\text{cent.}}(t)$.

In the range of small F_0 values, the electron transport through the device is characterized by transient regime towards a steady state with a dc and constant occupations as explained above. This is shown in Figs. 3(aa)–3(ac). For intermediate field strengths the onset of oscillations can be observed in both, the population dynamics, i.e., Fig. 3(ba), as well as in the time dependence of the partial currents, displayed in Figs. 3(bb) and 3(bc). Lastly, the lowermost triple block depicts data obtained for $F_0 = 0.2\gamma/a$. Here the oscillatory behavior acquires perfect sinusoidal form, as can be seen in Figs. 3(cb) and 3(cc). Comparing with the expression for the current obtained by a semiclassical analysis (see Appendix A), we find an excellent agreement.

The transition from dc to BOs regime can also be seen in the net current through the device $J_{\text{net}} \equiv (J_L - J_R)/2$. The latter is shown in Fig. 4, computed for each of the above field magnitudes. Namely, the upper plot in Fig. 4(a) captures the dc regime characterized by a nonvanishing J_{net} . In contrast, Figs. 4(b) and 4(c) show the emergence of BOs. Here, after

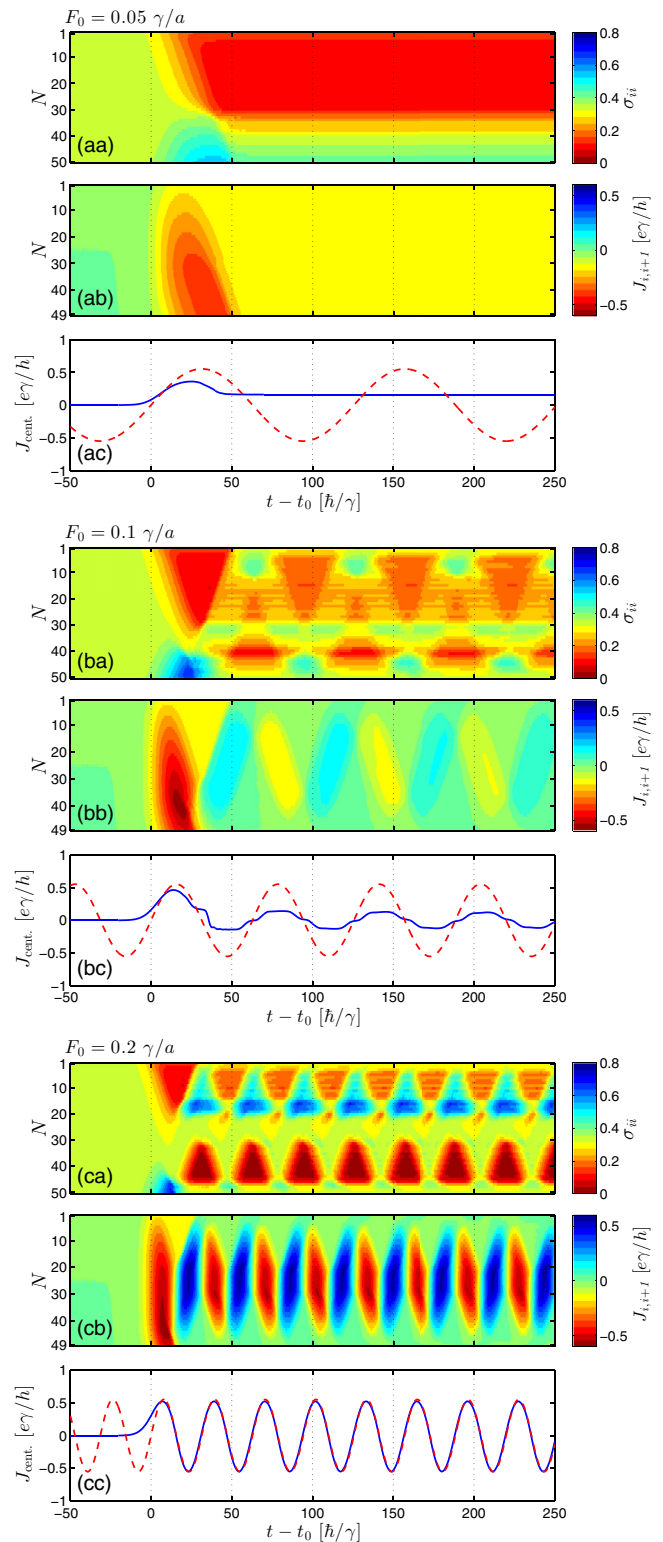


FIG. 3. Conceptually different transport regimes obtained by changing F_0 . (aa)–(ac) $F_0 = 0.05\gamma/a$: Typical transient relaxation to dc behavior. (ba)–(bc) $F_0 = 0.1\gamma/a$: Intermediate regime with onset of BOs. (ca)–(cc) $F_0 = 0.2\gamma/a$: Regime of BOs. For each of the triple blocks, the upper plot shows the occupation number, the middle one depicts the current between neighboring sites, and the lower plot displays the current in the center of the system $J_{\text{cent.}}(t)$. The system size is $N = 50$ in each case. The (red) dashed lines show the current according to Eq. (A4).

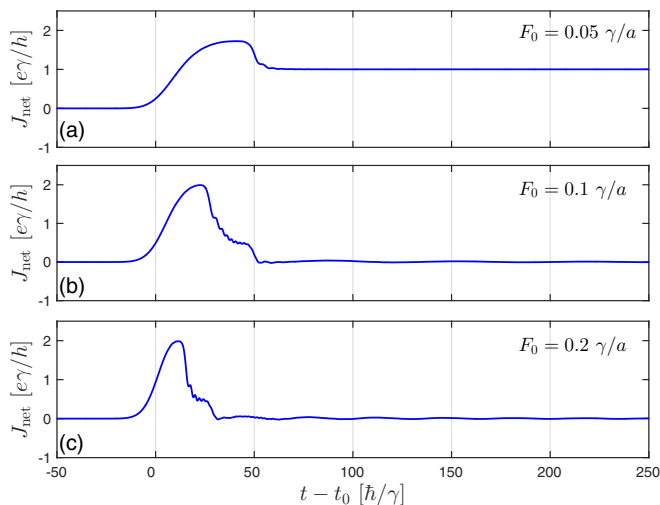


FIG. 4. Net current through the system ($N = 50$) for the three field magnitudes used for Fig. 3. (a) The transient transition towards a stationary state with nonvanishing dc current, while (b) and (c) correspond to the regime of BOs. In the latter regime, the net current vanishes.

the transient response to the switching of the field, the net current vanishes eventually. This situation corresponds to the occurrence of BOs seen in Fig. 3(cc).

C. Transferred charge

In an experimental setting the internal currents or the instantaneous occupation number are typically not directly measurable. While the data shown in the previous section clearly indicate the presence of two distinct transport regimes within the quantum system, it is desirable to visualize the pattern of BOs also in experimentally accessible observables. As we show in the following, a pump-probe scenario, where the rising flank of the pulse is used as a pump and the falling flank as a probe, can be utilized to investigate the internal dynamics. This approach has been, for example, successfully used for studying the dynamics of charge qubits in double quantum dots [35,36]. Accordingly, the time dependence of the electric field is explicitly given by $F(t) = F_0[\text{erf}[(t - t_0)/t_r] - \text{erf}[(t - t_0 - \tau)/t_r]]/2$, where τ is the pulse length. We calculate the charge injected into the right electrode, which is given by $Q(\tau) = -\int_{-\infty}^{\infty} dt' J_R(t')$, as a function of the pulse length [37].

In the dc regime, one expects $Q(\tau)$ to increase linearly with τ . This is confirmed by Fig. 5(a), which shows $Q(\tau)$ for the field-strength $F_0 = 0.03\gamma/a$. The transient response seen in Fig. 4(a) is only relevant for small $\tau < t_{\text{trans}} \approx 60\hbar/\gamma$, which is not shown here. On the other hand, in the BOs regime $Q(\tau)$ is entirely determined by the transient responses at the instants of switching on and off of the field. The switching-on contribution is the same for all $\tau > t_{\text{trans}}$ and leads to a constant offset. The switching-off contribution depends on the state of the system [36] and will thus be modulated by the BOs. This can be seen in Figs. 5(b) and 5(c) which show the pulse-length dependence of Q for $F_0 = 0.2\gamma/a$ and $F_0 = 0.4\gamma/a$. The accumulated charge can be well fitted by a sine function which has the period

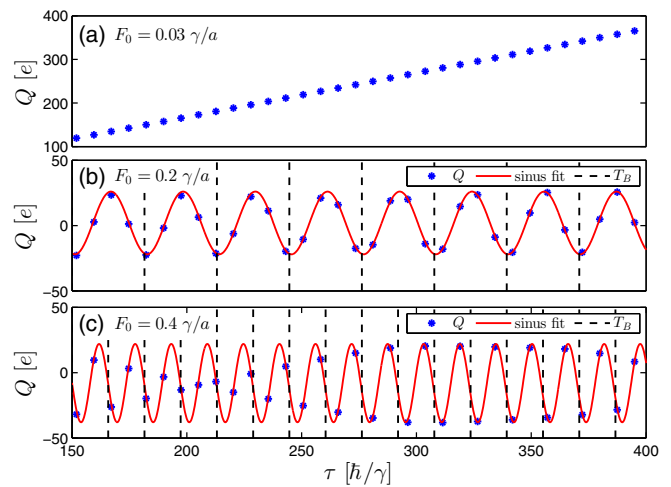


FIG. 5. Accumulated charge Q detected at the right electrode as function of pulse-length τ for three values of field strength F_0 corresponding to (a) direct current behavior and (b) and (c) BOs. For (b) and (c) the data points are fitted by a sine function (red curve). The vertical dashed lines mark the period of BOs.

T_B of the BOs. The amplitude of the oscillations depends on the state of the system around the instant of switching-off the pulse.

D. Effect of scattering

It is important to assess the effect of scattering from impurities on the overall formation of BOs, since impurity scattering is the main obstacle in directly detecting BOs in the current oscillations [38]. For this purpose, we phenomenologically introduce scattering by adding static disorder to the on-site energies ε_i . Specifically, we add to every on-site energy ε_i a random part $\Delta\varepsilon_i$ generated from a uniform distribution in the interval $[-w/2, w/2]$. We choose $w/2 = 0.15$ eV such that the localisation length remains larger than the system size (weak disorder limit [39]). Moreover, each calculation is performed with a fixed configuration. In Fig. 6 we show the current $J_{\text{cent.}}(t)$ averaged over 50 of such configurations. The simulation parameters are chosen as in Figs. 3(ca)–3(cc), which guarantees the emergence of BOs. We find the formed

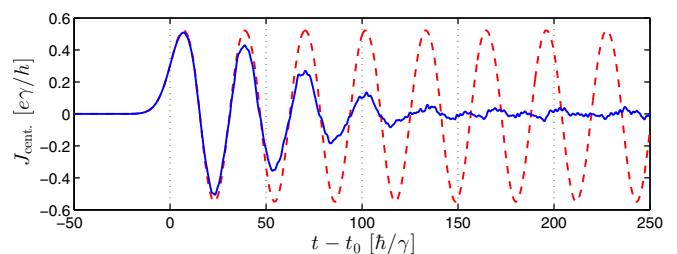


FIG. 6. Blue curve: current in the center of the system versus time for the parameters used in Figs. 3(ca)–3(cc). Scattering is accounted for by adding static disorder to the on-site energies. Data obtained as the average of 50 statistically independent configurations with disorder strength $w = 0.3\gamma$. The (red) dashed curve shows the current in the center of the system in the absence of scattering.

BOs to decay after a few periods (see Fig. 6). This result is in agreement with similar findings in the literature [8,38] and shows that our previous findings of Sec. III C remain valid also in the presence of scattering if, for instance, the pulse length used in Fig. 5 is shorter than the decay constant.

IV. CONCLUSIONS

In summary, we studied the emergence of BOs in paradigmatic 1D systems after switching on an external electric field. For small system sizes $N \ll L_B/a$, no BOs are observed and the stationary current is directed as expected. Increasing the system size beyond the Bloch-length L_B leads to the emergence of BOs, which are characterized by oscillating internal currents and a vanishing net current through the device. We find that the system size aN has to be larger than $2L_B$ to obtain BOs corresponding to the ones found in a homogeneous field. By employing a pump-probe scheme, which uses the rising and falling flanks of a nearly rectangular pulse, we showed that the BOs can be identified in the accumulated charge obtained as a function of pulse length. This offers a route to study dynamics of BOs and their interplay with noise and/or other degrees of freedom in nanoscale devices.

APPENDIX A: SEMICLASSICAL DESCRIPTION OF BOS

For an infinite system one can describe the electron dynamics using a semiclassical approach [23,40]. An electron is characterized by its position $x(t)$ and wave vector $k(t)$, which obey the equations of motion

$$\frac{\partial}{\partial t} x(t) = \frac{1}{\hbar} \frac{\partial \epsilon[k(t)]}{\partial k}, \quad \frac{\partial}{\partial t} k(t) = -\frac{1}{\hbar} F(t). \quad (\text{A1})$$

The band structure for the 1D tight-binding chain is $\epsilon(k) = -2\gamma \cos(ka)$. Before the electric field is switched on, the state $|k_0\rangle$ is occupied with probability $f[\epsilon(k_0)]$, where f is the Fermi function. After an instantaneous switching of the (homogeneous) electric field at time $t_0 = 0$ from zero to F_0 , one finds for the time dependence of x and k ,

$$x(t) = x_0 - \frac{2\gamma}{F_0} \cos(k_0 a) + \frac{2\gamma}{F_0} \cos[k_0 a - \omega_B t], \quad (\text{A2})$$

$$k(t) = k_0 - \frac{\omega_B}{a} t, \quad (\text{A3})$$

where $\omega_B = 2\pi/T_B$ is the Bloch frequency. Consequently, the current is given by

$$\begin{aligned} J(t) &= e \int_{-\pi/a}^{\pi/a} \frac{dk_0}{2\pi} f[\epsilon(k_0)] \left. \frac{\partial}{\partial t} x(t) \right|_{k(t)=k_0-\omega_B t/a} \\ &= -\frac{4e\gamma}{2\pi\hbar} \sin(k_F a) \sin(\omega_B t). \end{aligned} \quad (\text{A4})$$

In the last step above zero temperature was assumed and the Fermi wave vector k_F is related to the Fermi energy via $\epsilon_F = \epsilon(k_F)$.

APPENDIX B: SHORT SURVEY ON TDNEGF METHOD OF REF. [24]

The general time-dependent evolution of an open quantum system can be formulated in terms of the device Green's functions, which for the noninteracting case are given by

$$\mathbf{G}^r(t, t') = \mathbf{g}^r(t, t') + \int dt_1 \int dt_2 \mathbf{g}^r(t, t_1) \mathbf{\Sigma}^r(t_1, t_2) \mathbf{G}^r(t_2, t'), \quad (\text{B1})$$

$$\mathbf{G}^{\gtrless}(t, t') = \int dt_1 \int dt_2 \mathbf{G}^r(t, t_1) \mathbf{\Sigma}^{\gtrless}(t_1, t_2) \mathbf{G}^a(t_2, t'), \quad (\text{B2})$$

where \mathbf{G} and $\mathbf{\Sigma}$ are the standard two-time Green's functions and self-energies, respectively, with the superscripts \gtrless and r, a standing for greater/lesser and retarded/advanced. Note that the self-energies above contain contributions from all reservoirs. Moreover, \mathbf{g}^r designates the Green's function of the uncoupled device and satisfies

$$\left[i\hbar \frac{\partial}{\partial t} - \mathbf{H}_D(t) \right] \mathbf{g}^r(t, t') = \delta(t - t') \mathbf{1}. \quad (\text{B3})$$

Our approach [24,27] for dealing with Eqs. (B1)–(B3) uses the auxiliary quantities $\mathbf{\Pi}_\alpha(t)$, termed as current matrices, which are defined by

$$\mathbf{\Pi}_\alpha(t) = \int_{t_0}^t dt_2 [\mathbf{G}^>(t, t_2) \mathbf{\Sigma}_\alpha^<(t_2, t) - \mathbf{G}^<(t, t_2) \mathbf{\Sigma}_\alpha^>(t_2, t)]. \quad (\text{B4})$$

They serve at deriving [41] a compact equation for the RDO of the system [$\boldsymbol{\sigma}(t) \equiv \text{Im}\{\mathbf{G}^<(t, t)\}$], namely Eq. (2). Moreover, according to Eq. (3), the $\mathbf{\Pi}_\alpha$ matrices allow it to compute the current from lead α into the system.

In essence, the key ingredient of our approach [24,27] is the use of a parametrization for the level-width function $\Gamma_\alpha(\epsilon) \equiv -2\text{Im}\mathbf{\Sigma}^r(\epsilon)$ which allows it to express the greater/lesser two-time self-energies as a summation over weighted exponentials in time domain. This fact is then employed in deriving a set of closed ordinary differential equations (ODEs) for the current matrices $\mathbf{\Pi}_\alpha$ and also for the remanent term in their equations of motion. Moreover, in Ref. [24], in contrast to the original scheme of Ref. [27], we mapped the problem in terms of vectors instead of full matrices, to profit from the intrinsic sparseness of the latter for noninteracting systems. This leads to a significant reduction of computational effort, which then permits the full time-dependent treatment of larger systems.

[1] F. Bloch, *Z. Phys.* **52**, 555 (1929).

[2] C. Zener, *Proc. R. Soc. London* **145**, 523 (1934).

[3] M. Raizen, C. Salomon, and Q. Niu, *Phys. Today* **50**, 30 (1997).

[4] H. Ohno, E. E. Mendez, J. A. Brum, J. M. Hong, F. Agulló-Rueda, L. L. Chang, and L. Esaki, *Phys. Rev. Lett.* **64**, 2555 (1990).

- [5] C. Waschke, H. G. Roskos, R. Schwedler, K. Leo, H. Kurz, and K. Köhler, *Phys. Rev. Lett.* **70**, 3319 (1993).
- [6] V. G. Lyssenko, G. Valušis, F. Löser, T. Hasche, K. Leo, M. M. Dignam, and K. Köhler, *Phys. Rev. Lett.* **79**, 301 (1997).
- [7] P. Leisching, P. Haring Bolivar, W. Beck, Y. Dhaibi, F. Brüggemann, R. Schwedler, H. Kurz, K. Leo, and K. Kohler, *Phys. Rev. B* **50**, 14389 (1994).
- [8] G. von Plessen, T. Meier, J. Feldmann, E. C. Göbel, P. Thomas, K. W. Goossen, J. M. Kuo, and R. F. Kopf, *Phys. Rev. B* **49**, 14058(R) (1994).
- [9] M. Ben Dahan, E. Peik, J. Reichel, Y. Castin, and C. Salomon, *Phys. Rev. Lett.* **76**, 4508 (1996).
- [10] S. R. Wilkinson, C. F. Bharucha, K. W. Madison, Q. Niu, and M. G. Raizen, *Phys. Rev. Lett.* **76**, 4512 (1996).
- [11] B. P. Anderson and M. A. Kasevich, *Science* **282**, 1686 (1998).
- [12] T. Pertsch, P. Dannberg, W. Elflein, A. Bräuer, and F. Lederer, *Phys. Rev. Lett.* **83**, 4752 (1999).
- [13] R. Morandotti, U. Peschel, J. S. Aitchison, H. S. Eisenberg, and Y. Silberberg, *Phys. Rev. Lett.* **83**, 4756 (1999).
- [14] R. Sapienza, P. Costantino, D. Wiersma, M. Ghulinyan, C. J. Oton, and L. Pavesi, *Phys. Rev. Lett.* **91**, 263902 (2003).
- [15] F. Domínguez-Adame, V. A. Malyshev, F. A. B. F. de Moura, and M. L. Lyra, *Phys. Rev. Lett.* **91**, 197402 (2003).
- [16] S. Longhi, *Phys. Rev. B* **81**, 195118 (2010).
- [17] M. Holthaus, *Phys. Rev. Lett.* **69**, 351 (1992).
- [18] J. Rotvig, A.-P. Jauho, and H. Smith, *Phys. Rev. Lett.* **74**, 1831 (1995).
- [19] A. Buchleitner and A. R. Kolovsky, *Phys. Rev. Lett.* **91**, 253002 (2003).
- [20] T. Schulte, S. Drenkelforth, G. K. Büning, W. Ertmer, J. Arlt, M. Lewenstein, and L. Santos, *Phys. Rev. A* **77**, 023610 (2008).
- [21] S. Longhi, *Phys. Rev. B* **86**, 075144 (2012).
- [22] L. da Silva, M. Sales, A. R. Neto, M. Lyra, and F. de Moura, *Solid State Commun.* **248**, 123 (2016).
- [23] T. Hartmann, F. Keck, H. J. Korsch, and S. Mossmann, *New J. Phys.* **6**, 2 (2004).
- [24] B. S. Popescu and A. Croy, *New J. Phys.* **18**, 093044 (2016).
- [25] A.-P. Jauho, N. S. Wingreen, and Y. Meir, *Phys. Rev. B* **50**, 5528 (1994).
- [26] H. Haug and A.-P. Jauho, *Quantum Kinetics in Transport and Optics of Semiconductors* (Springer, Berlin, 1996).
- [27] A. Croy and U. Saalman, *Phys. Rev. B* **80**, 245311 (2009).
- [28] B. Popescu, P. B. Woiczikowski, M. Elstner, and U. Kleinekathofer, *Phys. Rev. Lett.* **109**, 176802 (2012).
- [29] S. G. Chen, Y. Zhang, S. Koo, H. Tian, C. Y. Yam, G. H. Chen, and M. Ratner, *J. Phys. Chem. Lett.* **5**, 2748 (2014).
- [30] H. Xie, Y. Kwok, Y. Zhang, F. Jiang, X. Zheng, Y. Yan, and G. Chen, *Phys. Status Solidi B* **250**, 2481 (2013).
- [31] H. Cao, M. Zhang, T. Tao, M. Song, and C. Zhang, *J. Chem. Phys.* **142**, 084705 (2015).
- [32] R. Wang, D. Hou, and X. Zheng, *Phys. Rev. B* **88**, 205126 (2013).
- [33] A. Croy, U. Saalman, A. R. Hernandez, and C. H. Lewenkopf, *Phys. Rev. B* **85**, 035309 (2012).
- [34] A. Croy and U. Saalman, *Phys. Rev. B* **86**, 035330 (2012).
- [35] T. Hayashi, T. Fujisawa, H. D. Cheong, Y. H. Jeong, and Y. Hirayama, *Phys. Rev. Lett.* **91**, 226804 (2003).
- [36] A. Croy and U. Saalman, *New J. Phys.* **13**, 043015 (2011).
- [37] In practice the integration starts from the beginning of the simulation.
- [38] E. Diez, F. Domínguez Adame, and A. Sánchez, *Microelectron. Eng.* **43-44**, 117 (1998).
- [39] D. J. Thouless, in *Ill-condensed Matter*, edited by G. Toulouse and R. Balian (North-Holland, Amsterdam, 1979), pp. 1–62.
- [40] N. W. Ashcroft and N. D. Mermin, *Solid State Physics* (Holt, Rinehart and Winston, New York, 1976).
- [41] X. Zheng, F. Wang, C. Y. Yam, Y. Mo, and G. H. Chen, *Phys. Rev. B* **75**, 195127 (2007).